Monitoring Observations of SMC X-1's Excursions (MOOSE) I: Program Description and Initial High-State Spectral Results

Kristen C. Dage[1,2]* McKinley Brumback,[3] Joey Neilsen, [4] Chin-Ping Hu,[5]

Diego Altamirano,[6] Arash Bahramian,[7] Philip A. Charles [6] William I. Clarkson,[8]

Daryl Haggard,[1,2] Ryan C. Hickox,[9] Jamie Kennea[10]

[1]*Department of Physics, McGill University, 3600 University Street, Montréal, QC H3A 2T8, Canada*
[2]*McGill Space Institute, McGill University, 3550 University Street, Montréal, QC H3A 2A7, Canada*
[3] *Cahill Center for Astronomy and Astrophysics, California Institute of Technology, 1216 E California Blvd, Pasadena, CA 91125, USA*
[4] *Villanova University, Department of Physics, Villanova, PA 19085, USA;*
[5] *Department of Physics, National Changhua University of Education, Changhua, 50007, Taiwan*
[6]*Physics & Astronomy, University of Southampton, Southampton, Hampshire SO17 1BJ, UK*
[7]*International Centre for Radio Astronomy Research − Curtin University, GPO Box U1987, Perth, WA 6845, Australia*
[8]*Department of Natural Sciences, University of Michigan-Dearborn, 4901 Evergreen Rd. Dearborn, MI, 48128*
[9] *Department of Physics & Astronomy, Dartmouth College, 6127 Wilder Laboratory, Hanover, NH 03755, USA*
[10] *Department of Astronomy and Astrophysics, The Pennsylvania State University, University Park, PA 16802, USA*

ABSTRACT

SMC X-1 has exhibited three super-orbital period excursions since the onset of X-ray monitoring beginning with RXTE's launch in 1995. NICER has recently probed a fourth observed excursion beginning in 2021 with our program Monitoring Observations of SMC X-1's Excursions (MOOSE). These sensitive new MOOSE data probe different super-orbital periods and phases within them. Spectral fits to the high-state continuum during April 2021 to January 2022 show that the intrinsic spectral shapes are characterised by a soft (kT~0.19 keV) disc component and a hard (Γ ~0.7) power-law tail. When the 2021-2022 NICER observations, taken during an excursion, are compared to 2016 XMM-Newton observations (outside of an excursion), we find little evidence for intrinsic spectral variability across the high-states, but find evidence for a $>3~\sigma$ change in the absorption, although we caution that there may be calibration differences between the two instruments. Thus, over different lengths of super-orbital periods, we see little evidence for intrinsic spectral changes in the high-state. Upcoming studies of the pulse profiles may shed light on the mechanism behind the excursions.

Key words: accretion, accretion discs – stars: pulsars: individual: SMC X-1 – X-rays: binaries

1 INTRODUCTION

Modulation in X-ray binary lightcurves has long been used as a diagnostic to understand key physical processes in the system. One such modulation that has garnered interest over the last ~50 years are observations of super-orbital periodicities.

Super-orbital periods−− the detection of a periodicity in an X-ray binary which is longer than the orbital period of the binary− have been significantly detected in many different types of systems. These include supergiant fast X-ray transients, wind-accretion systems, as well as persistent (Roche lobe overflow), high-mass X-ray binaries and low-mass X-ray binaries with both black hole and neutron star primaries (Kotze & Charles 2012; Corbet & Krimm 2013). Recent optical studies also showed evidence for super-orbital periodicites in the black hole transient MAXI J1820+070 (Thomas et al. 2022).

One explanation is that super-orbital period modulation is due to a warped, precessing accretion disc that is observed edge-on, such that the disc obscures the accretor during precession Clarkson et al.

(2003b). As such, the super-orbital period is a direct observable of the accretion disc configuration. For systems like the neutron star X-ray binary SMC X-1, one generally accepted cause of warps in X-ray binary accretion discs is radiation driven warping (Pringle 1996; Ogilvie & Dubus 2001). The stability of the warped disc structure is determined by binary parameters such as radius and mass ratio (e.g. Clarkson et al. 2003a,b). In systems that do not fall in the stability range, like SMC X-1, fluctuations in the geometry of the accretion disc can be observed as fluctuations in super-orbital behaviour (Ogilvie & Dubus 2001).

SMC X-1 is a well-studied high mass X-ray binary with a known neutron star accretor and a B0 I supergiant companion (Reynolds et al. 1993), The system has a 3.89 day orbital period (Schreier et al. 1972) and the neutron star produces a ∼ 0.7s pulse period (Lucke et al. 1976), which, since the 1970s, its ∼ 0.7 s pulse period has steadily been spun up (Inam et al. 2010). Hu et al. (2019) report the spin-up frequency derivative as ∼ 2.5 ×10^{-11} s^{-2}. Early studies of SMC X-1's X-ray spectral properties identified both hard and soft spectral components (Marshall et al. 1983). These components likely originate from different physical processes (Naik & Paul 2004).

* E-mail: kristen.dage@mcgill.ca

Hickox & Vrtilek (2005) modeled the hard and soft emission with a twisted inner disc, which indicated that the hard emission may be due to the illuminating pulsar beam, and the soft component caused by the reprocessed emission of the inner accretion disc.

SMC X-1 is also well known for its super-orbital period, which is typically measured close to 60 days, but can take excursions to periods as low as 45 days (Clarkson et al. 2003a; Dage et al. 2019; Hu et al. 2019). The characterisation and physical origins of the super-orbital period (P_{sup}) modulation have been the subject of many studies over the last few decades (see, e.g. Gruber & Rothschild 1984; Wojdowski et al. 1998; Clarkson et al. 2003a; Trowbridge et al. 2007; Hu et al. 2011, 2013; Dage et al. 2019; Hu et al. 2019, and references therein), with many techniques implemented to accurately measure these long-term modulations, including dynamical power spectrum and Hilbert-Huang (Huang et al. 1998) transform analysis.

Spectral studies by Wojdowski et al. (2000) determined that the spectral properties are at odds with predictions from line-driven wind models (Blondin & Woo 1995). RXTE spectral monitoring by Inam et al. (2010) found little evidence of spectral variation, except that N_H increased as the X-ray flux dropped, and monitoring of the spectrum by Vrtilek et al. (2005) showed that the super-orbital period cycle influences the spectrum, as the low state spectra were linked to the orbital phase, but not the high state spectra. The role that radiation-driven warping plays in SMC X-1's super-orbital period is very much a mystery, as recent analysis by Pradhan et al. (2020) suggests that a warped accretion disk is not the only cause of P_{sup}, but variability in the power-law normalization could imply that intrinsic changes from the source itself are a factor in producing the observed super-orbital periodicity.

Other tests to determine the geometry of the disc can also be probed via studies of the pulse profiles: variation in the soft pulse profiles may be related to precession in the disc (Neilsen et al. 2004). Brumback et al. (2020) implemented X-ray tomography techniques to directly model the warped accretion disc, in particular, the inner part near the magnetosphere, and showed that the direct (hard) pulse profile and reprocessed (soft) pulse profile can both be separately traced by X-ray spectra. The hard and soft pulse profile offsets changed within a given 60 day super-orbital period cycle, but the pulse profiles at the beginning and end of the 60 day cycle were almost identical– implying that the inner accretion disc had completed an entire precessed cycle.

Observational and theoretical tests can be made to determine if SMC X-1's disc warp and roving super-orbital period is attributed to radiation driven warping, where irradiation from a central source warps the accretion disc. Smoothed particle hydrodynamical simulations by Foulkes et al. (2006, 2010) suggest this is quite possible. Such a scenario would imply a link between the *change* in super-orbital period and the mass transfer rate. Dage et al. (2019) searched for such a link, but they were not able to find conclusive observable evidence. Hu et al. (2019)'s complete analysis of the super-orbital period from 1999-2019, along with analysis of spin periods thanks to *MAXI GSC* found no evidence that the mass transfer rate was strongly associated with the super-orbital period, but suggested that the super-orbital period modulation could be due to a torque change (which in turn is dependent on the mass transfer rate and the warp angle).

Understanding the nature of SMC X-1's warped, precessing accretion disc has risen to greater importance with the discovery of the pulsating ultraluminous X-ray sources (ULXPs; e.g., Bachetti et al. (2014)). SMC X-1 may be a nearby analog to the ULXPs, as it also exhibits pulse dropouts (Pike et al. 2019; Bachetti et al. 2020). Many ULXs are now thought to exhibit super-orbital periods and possibly also accretion disc warping (see, e.g., Motch et al. 2014; Brightman et al. 2019; Walton et al. 2016, among others), see also Townsend & Charles (2020) and references therein. Understanding SMC X-1's super-orbital behaviour can shed light on the mysterious, and more distant ULXPs, as well as provide a unique understanding on the physical processes responsible for X-ray binary variability on many timescales.

Our *NICER* observing program, **M**onitoring **O**bservations **Of** **S**MC X-1's **E**xcursions (MOOSE) is designed to fully utilise *NICER*'s monitoring capabilities to provide information on SMC X-1's spectral shape and soft timing properties as the sources enters a new state of super-orbital period modulation. These properties have not yet been probed during an epoch of super-orbital period excursion, and MOOSE will provide a rich and diverse data-set to shed light on the physical properties of the system during this time. This paper is the first in the series focusing on the high-state spectra. Detailed timing analysis of the system will be presented in Brumback et al. (in prep). In Section 2.1 we describe the MOOSE campaign; Section 2 discusses initial spectral analysis. These results are discussed in Section 3, while Section 4 considers the next steps to be undertaken in the analysis of MOOSE's dataset.

2 DATA AND ANALYSIS

NICER's superb timing resolution (<300 nsec) and monitoring capabilities, along with sensitivity in the soft (0.2-12 keV) energy range (Gendreau et al. 2016) present an excellent opportunity to study SMC X-1 throughout the duration of the newest super-orbital period excursions. The observations are spaced roughly 10 days apart, and sample different stages of the super-orbital cycle. The data quality is a function of the observation length and the phase of the super-orbital cycle that is observed (as observations taken in the low state have a much lower count rate). Figure 1 shows the observations plotted against the *Swift*/BAT monitoring lightcurve, with each observation flagged by data quality.

As discussed in Section 2.2, the super-orbital cycles are not consistent with each other for the duration of the monitoring interval (see also Figure 2).

2.1 Data Reduction and Reprocessing

The *NICER* observations were processed with HEAsoft 6.29 NICERL2 task, with the overonly range extended to 1.5, as the overonly ranges of many of the data often exceeded this value (see Table 1). Overshoots (the overonly range) measure the high energy particle backgrounds, while undershoots (the underonly range) are detector resets which measure red noise and any optical light. [1] The spectra were extracted with XSELECT, and we implemented optimal binning [2] with no minimum number of counts (Kaastra & Bleeker 2016). The background spectra were generated using the NIBACKGEN3C50 tool (Remillard et al. 2021), and we used the NICERARF and NICERRMF tasks to generate individual ARF and RMF files for each spectrum.

---

[1] https://heasarc.gsfc.nasa.gov/docs/nicer/data_analysis/
workshops/NICER-Workshop-Filtering-Markwardt-2021.pdf
[2] https://heasarc.gsfc.nasa.gov/docs/nicer/analysis_
threads/spectrum-grouping/
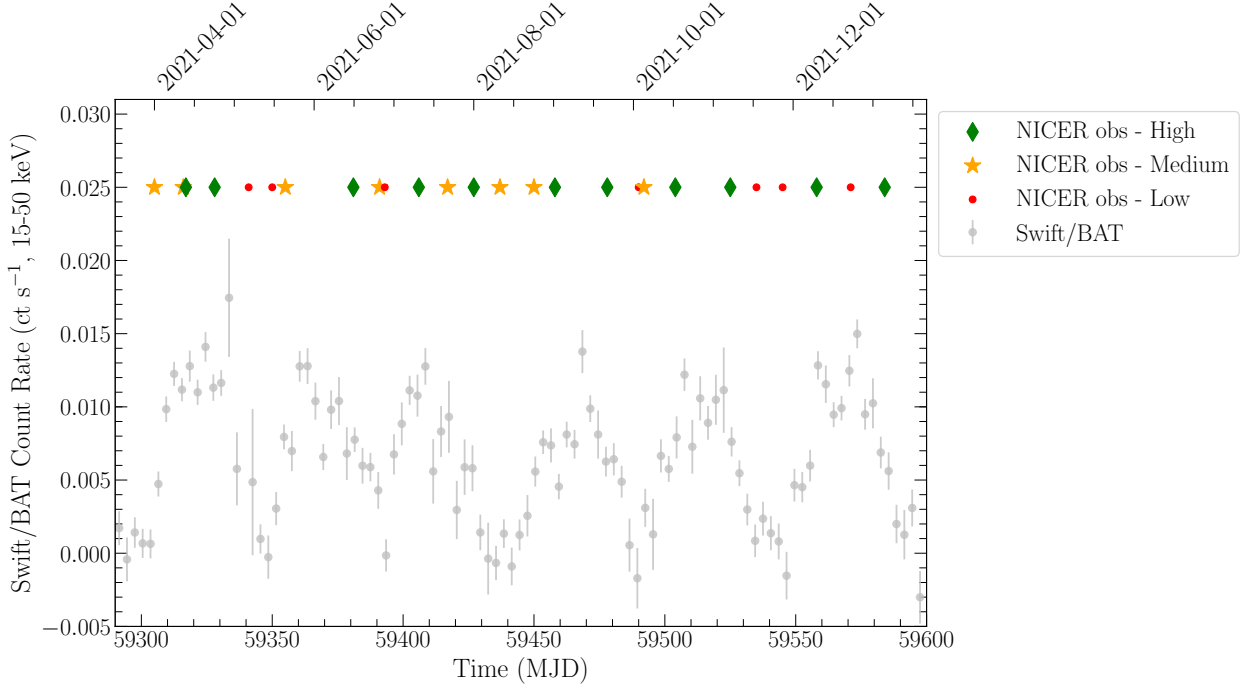
Figure 1. Rebinned *Swift*/BAT monitoring of SMC X-1 overlaid with observation times from the *NICER* monitoring campaign. Each observation is differentiated by data quality (green diamond are the highest count rates, yellow star is intermediate, red dot is the lowest), which is a function of observation length and where within the super-orbital period cycle the snapshot was taken.

Table 1. *NICER* observations log.

ObsID	Date	Duration (sec)	Overonly Range	Underonly Range (ct/sec)	Count Rate
4509012401	2022-01-05	1474	<15	<300	151
4509012301	2021-12-23	2411	<1	<306	5
4509012201	2021-12-10	1476	<11	<200	249
4509012101	2021-11-27	1513	<100	<200	6
4509012001	2021-11-17	955	<75	<200	10
4509011901	2021-11-07	1259	<30	<200	176
4509011701	2021-10-17	2533	<1	<200	195
4509011601	2021-10-05	1107	<10	<200	10
4509011501	2021-10-03	350	<16	<200	9
4509011401	2021-09-21	1476	<35	<200	245
4509011301	2021-09-01	1898	<0.5	<200	189
4509011201	2021-08-24	1327	<20	<200	52
4509011101	2021-08-11	1123	<1	<200	9
4509011001	2021-08-01	1235	<50	<200	72
4509010901	2021-07-22	821	<20	<200	179
4509010803	2021-07-11	944	<30	<200	232
4509010802	2021-06-28	796	<20	<200	10
4509010801	2021-06-26	1684	<1.5	<200	139
4509010701	2021-06-16	1279	<2	<200	206
4509010601	2021-05-21	1024	<4	<200	146
4509010501	2021-05-16	1446	<140	<200	7
4509010401	2021-05-07	967	<40	<200	2
4509010301	2021-04-24	436	<20	<200	195
4509010103	2021-04-13	483	<7	<200	220
4509010102	2021-04-12	1362	<3	<200	214
4509010101	2020-04-01	1006	<11	<200	33

2.2 Determining changes in P_{sup} from BAT monitoring

SMC X-1 has been observed to undergo three separate epochs of super-orbital period excursion, which last for 2-3 years, occurring in 1997, 2006, and 2014 (Hu et al. 2019). While it is difficult to accurately predict the onset of the next super-orbital period excursion, the ∼ 6 year difference gap between previous super-orbital period excursions suggested that SMC X-1 would undergo some type of super-orbital period excursion beginning in 2021.

Most techniques to perform accurate measurements of super-orbital periodicities, such as the Lomb-Scargle periodogram (Scargle 1982) often require hundreds of days worth of data to perform a single period measurement. While there is always a concern that red noise can cause problematic false detections (Vaughan et al. 2016), SMC X-1's super-orbital period is well-known and has been observed with many repetitions.

Given that our monitoring campaign has not yet exceeded one year and is comprised of short observations with days-long gaps, techniques such as the Lomb-Scargle periodogram are not the most effective methods to constrain the super-orbital period. However, phase dispersion minimization is one of the techniques enabling us to measure periods from these data sets.

To quantify any super-orbital period changes between the 2016 and 2021 epochs, we implement the python package P4J, where the criterion for period detection is based on maximizing the Cauchy-Schwarz Quadratic Mutual Information (Huijse et al. 2018) [3] to measure the best super-orbital period of the BAT data taken from MJD 59290-59606, which covers 5 super-orbital cycles (we removed the cycle before MJD 59290 because the data gap was problematic), and interpolated a sine model from the best fit period (P_{sup}=51d). For comparison, we implemented the same methodology on 5 cycles of the BAT data from MJD 57535-57788 (during the time the comparison *XMM-Newton* observations were taken). P4J returned the best fit period of 53 days, and the 2016 cycles appear to be self-consistent. We superimpose these models over-top the *Swift*/BAT monitoring in Figure 2. While the *XMM-Newton* epoch can be represented by a sinusoidal model with the period derived from P4J, the *NICER* epoch cannot all be fit by the modeled P4J period for that epoch, which implies that the super-orbital period is not a constant value during this time. This suggests that the MOOSE data set is unique because it provides both spectral and timing windows into unprobed regimes of P_{sup} for SMC X-1.

2.3 Monitoring of the High-State Continuum during the excursion

As an initial step to monitor the continuum, we fit spectra of the high-state observations using xspec version 12.12.0, with solar abundances from Wilms et al. (2000) and χ^2 statistics, with photo-electric absorption cross-sections from Verner et al. (1996). All reported uncertainties are at 90% confidence, and we implemented optimal binning [4]. The high-state observations can be described by the model tbabs*(bbody+cutoffpl) with three gaussian components added to model emission lines (see Figure 3). We restricted the search range of the high-energy cut-off value between 12 keV and 20keV to allow the fits to more closely match Brumback et al. (2020). While *NICER* does not extend to this range, the inclusion of a hard

component is necessary to fit the spectrum. SMC X-1 is known to produce emission from Fe Kα (6.4 keV, broad), Ne X Lyα (1.2 keV), and O VIII Lyα (0.65 keV), and we fix our emission lines to the same line energy and width as Brumback et al. (2020). The low/intermediate state spectra are not well-fit by this model. We will undertake a comprehensive examination of all of the low/intermediate state data once the full MOOSE dataset has been acquired.

For comparison, we fit the same models to the high state *XMM-Newton* observations from Brumback et al. (2020) (ObsIDs 0784570201, 0784570301, 0784570501; see Brumback et al. 2020 for analysis details), which were obtained in 2016 when the source was not in a state of super-orbital period modulation.

The best-fit parameters for N_H, kT and Γ are presented in Table 2 and can be seen in Figure 4. We note that given the spectral resolution of *XMM-Newton*, the models we use are likely over-simplistic, however, we use the same models for *XMM-Newton* and *NICER* for sake of consistency and ease of comparison across the epochs.

3 RESULTS AND DISCUSSION

We fit *XMM-Newton* and *NICER* high state spectra of SMC X-1 through different P_{sup} values and phases and find no significant spectral changes, except for an apparent moderate variability in Γ. As the best-fit value for Γ depends on the high-energy cut-off, a parameter *NICER* is not sensitive to (as the best-fit values are sometimes outside the NICER energy range), we cannot yet conclude whether it is variable or not. As seen in Figure 4, the best-fit N_H increases between the XMM-Newton and *NICER* observations (from an average *XMM-Newton* value of 2.1 (+/- 0.08) $\times 10^{21}$ cm^{-2} to an average *NICER* value 2.5 ($\pm$ 0.01)$\times 10^{21}$ cm^{-2}). However, the temperature remains relatively stable with both *XMM-Newton* and *NICER* giving an average kT of 0.20 keV to a precision of <0.04 keV.

There appears to be slight variability in Γ, although that may be due to a degeneracy with the high-energy cut-off parameter, which *NICER* is not sensitive to (see next section and Fig 5). Thus, this study cannot comment on any potential variability of the power-law index. Our observations show that the overall spectral shape remains remarkably steady across the different superorbital modulations and phases covered here.

3.1 Comparison to Previous Spectral Studies of SMC X-1

Some comparisons can be made between spectral fits to the MOOSE high-state observations and SMC X-1 spectral fits from the literature. In particular, Naik & Paul (2004) observed SMC X-1 with *BeppoSAX* while SMC X-1 was in the onset of the first observed super-orbital period excursion (early 1997). Their spectra contained similar features to *ASCA* observations from Paul et al. (2002): a 6.4 keV iron emission line, a power-law component and a soft excess. However, the BeppoSAX observations were not sufficiently long enough to place constraints on variation in the soft excess between Paul et al. (2002) and Naik & Paul (2004). We find that the MOOSE observations have the same features, and remarkably similar X-ray fits (over the same energy ranges) across several years and different instruments, e.g. Naik & Paul (2004), yielding soft component kT values between 0.16-0.19 keV. Fits by Brumback et al. (2020) find that within different super-orbital phases, the overall spectral shape of the high-state remains similar, with any changes occurring in the normalization of the Fe line, or small differences in the primary power-law index.

The hard bands of SMC X-1 have also been observed many times, with *RXTE*, *Suzaku* and *NuSTAR*: Inam et al. (2010) fit *RXTE*/PCA

---

[3] https://github.com/phuijse/P4J
[4] https://heasarc.gsfc.nasa.gov/docs/nicer/analysis_threads/spectrum-grouping/
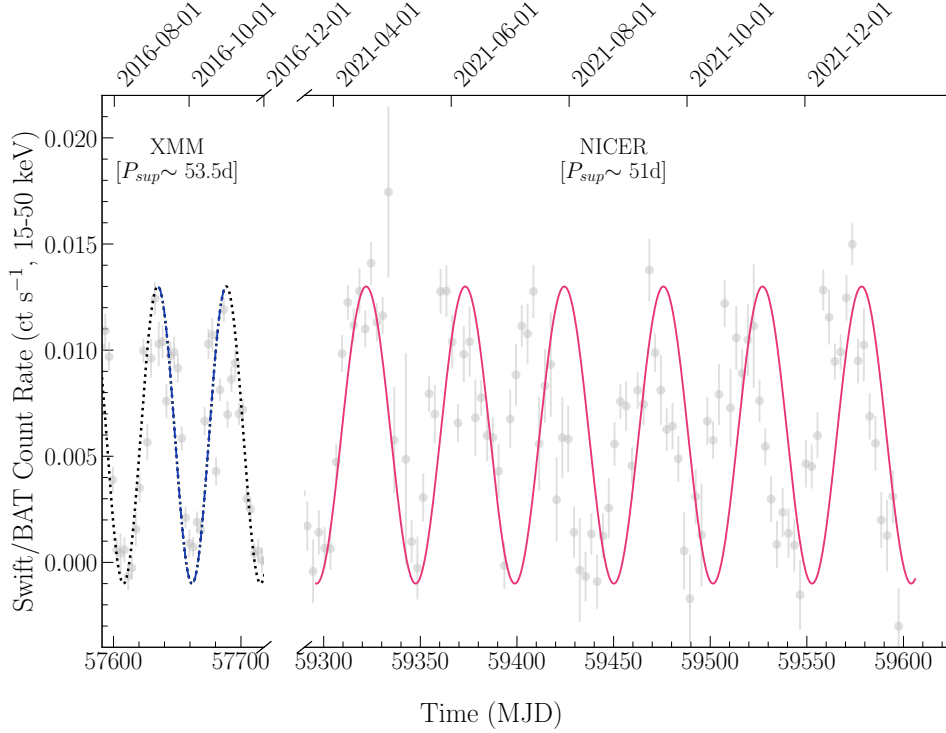
Figure 2. Comparison of the super-orbital period cycle during the 2016 *XMM-Newton* observations and the current *NICER* monitoring campaign. We fit the two different epochs of *Swift*/BAT observations with P4J and overlay the model with best-fit parameters on the image. The dashed blue lines on the left panel are the cycle that was observed by *XMM-Newton*, while the dotted lines show the best-fit period over the whole data-set used to measure the period. The left panel shows the P4J model during the *NICER* monitoring.

Table 2. Best-fit spectral parameters for high-state observations from each super-orbital period epoch. The *NICER* and *XMM-Newton* observations are fit in the 0.3-12 keV energy range.

ObsID	Date	$N_{\rm H}$ (10^{21}cm^{-2})	kT (keV)	Γ	χ^2 /d.o.f.
07845770201	2016-09-08	2.02 ± 0.05	0.197 ± 0.002	0.569 ± 0.021	1043.28/208
07845770301	2016-09-19	2.02 ± 0.06	0.198 ± 0.003	0.603 ± 0.026	888.42/206
07845770501	2016-10-24	2.1 ± 0.04	0.195 ± 0.002	0.63 ± 0.018	2026.07/216
4509010103	2021-04-13	2.4 ± 0.1	0.20 ± 0.01	0.75 ± 0.11	172.35/138
4509010301	2021-04-24	2.6 ± 0.1	0.19 ± 0.01	$0.58\ 0.11$	152.06/134
4509010701	2021-06-16	2.4 ± 0.1	0.20 ± 0.01	0.63 ± 0.07	286.20 /153
4509010803	2021-07-11	2.5 ± 0.1	0.20 ± 0.01	0.73 ± 0.08	191.66/150
4509010901	2021-08-01	2.4 ± 0.1	0.19 ± 0.01	0.66 ± 0.08	198.70/147
4509011301	2021-09-01	2.4 ± 0.1	0.20 ± 0.01	0.61 ± 0.01	211.42 /153
4509011401	2021-09-21	2.5 ± 0.1	0.19 ± 0.01	0.78 ± 0.07	272.90/152
4509011701	2021-10-17	2.5 ± 0.1	0.20 ± 0.01	0.66 ± 0.05	299.49/151
4509011901	2021-11-07	2.5 ± 0.1	0.20 ± 0.01	0.67 ± 0.05	196.29/145
4509012201	2021-12-10	2.4 ± 0.1	0.20 ± 0.01	0.73 ± 0.07	239.19/150
4509012401	2022-01-05	2.7 ± 0.1	0.19 ± 0.01	0.75 ± 0.03	208.44/138

(3-25 keV) observations with a cutoff power-law only, but find that the only parameter that changes within the error-bars is $N_{\rm H}$, which is anti-correlated to the X-ray flux. Fits by Pike et al. (2019) found that the spectrum in the low-state was poorly constrained due to the low number of source counts, and that a low-temperature (kT< 0.5 keV) component was necessary to model excess soft flux. This component was not recovered by Pradhan et al. (2020) fits to *Suzaku* and *NuStar* spectra, but they did find evidence for the hard X-ray spectrum becoming steeper as the flux increased.

While we do detect some changes in the best fit values for $N_{\rm H}$ between the 2016 *XMM-Newton* observations and the 2021-2022 *NICER* observations, it is not clear at this point whether the differ-

ences are due to calibration (see Brumback et al. 2020 for more detail on the *XMM-Newton* observations), or potential disc changes during excursion. Γ also appears to show some variance within the *NICER* observations. However, we note that there is a degeneracy between the best-fit value for the high-energy cut-off, which extends beyond *NICER*'s energy range, and thus it is not clear whether the power-law index shows intrinsic variability, or rather if the fit was not well constrained (see Figure 5). Thus, this study is not well-equipped to comment on variability in the power-law index.
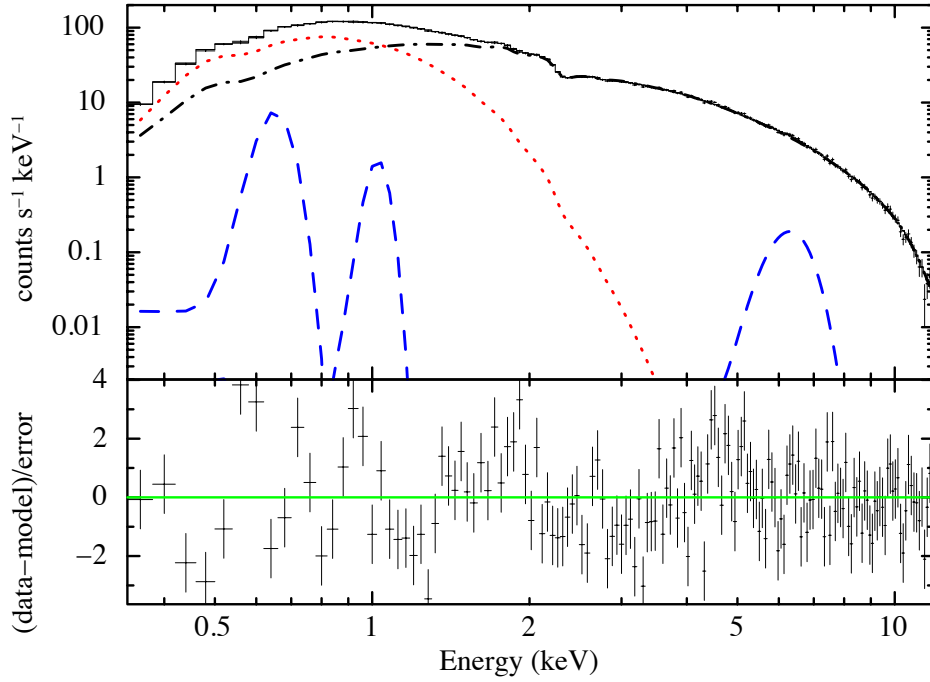
Figure 3. Best-fit spectrum and residuals of ObsID 4509011701. The spectrum was fit with tbabs*(bbody+cutoffpl+gaussian+gaussian+gaussian). The Gaussian components for line energy and σ were fixed to the values from Brumback et al. (2020). The xspec model components are as follows: bbody (red dotted line), cutoffpl (black dash-dotted line), and the three Gaussian components (blue dashed line). The uncertainties in the *XMM-Newton* observations are likely underestimated given the high reduced χ^2 values.
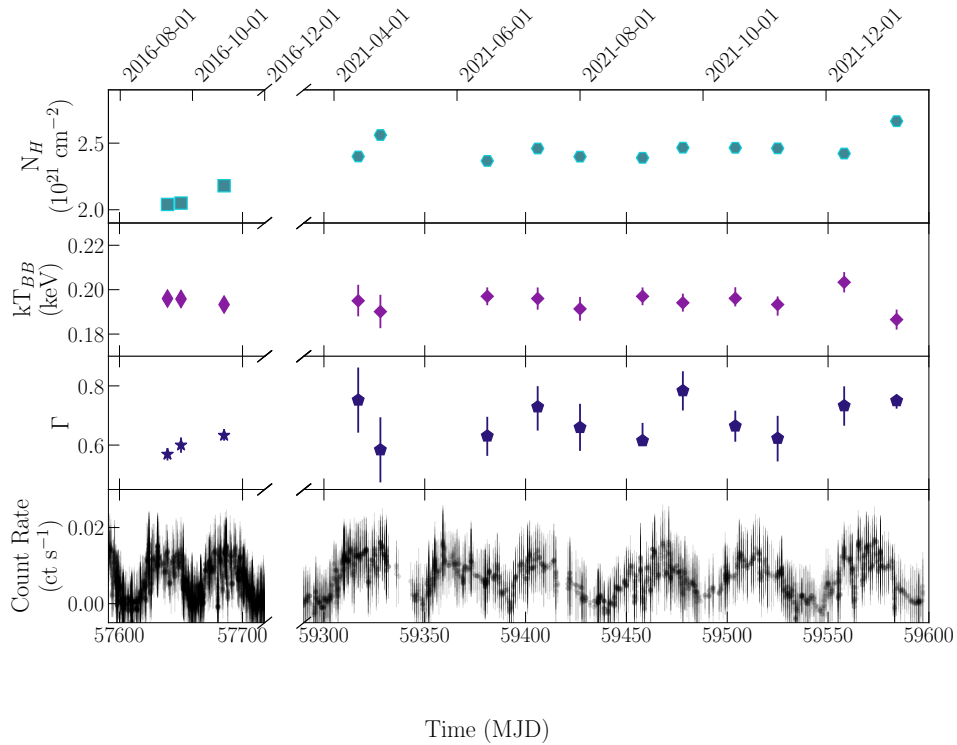
Figure 4. Best-fit parameters of $N_{\rm H}$, kT and Γ for high-state observations, with *Swift*/BAT light curve for reference. These parameters can be found in Table 2.
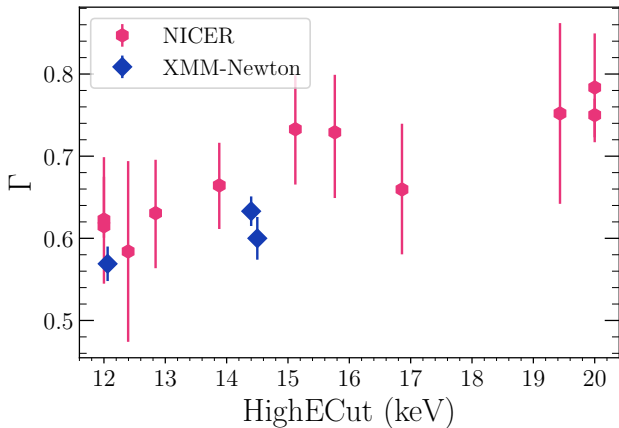
Figure 5. Best fit power-law index compared to best fit high energy cut value. *NICER* is not sensitive to the same energy ranges as *XMM-Newton*, and thus had a wider range of best-fit values for the high energy cut, which in turn impacted the corresponding value for the power-law index.

3.2 Comparison of SMC X-1 to ULX Pulsars with Super-Orbital Periods

SMC X-1 is known to reach high X-ray luminosities that are consistent with being near or above its Eddington limit (for a 1.1 solar mass NS; Bonnet-Bidaud & van der Klis (1981); Van der Meer et al. (2007); Pike et al. (2019). The richness of observational data on SMC X-1 makes it an ideal target for comparison with extragalactic ultraluminous X-ray pulsars, as several have been found to exhibit evidence for super-orbital periodicities, including NGC 7793 P13; (Motch et al. 2014), NGC 5907 ULX1; (Walton et al. 2016), M82 X-2; (Brightman et al. 2019), M51 ULX7; (Brightman et al. 2020). Due to the distance of these galaxies, it is challenging to perform detailed measurements of the pulse profiles, and thus the main observables utilised to understand these systems are the spectral shape and spectral evolution. Thus, it is potentially useful to be able to compare the long-term monitoring of SMC X-1's spectral behaviour to studies of these systems.

While it is challenging to perform spectral studies of M82 X-2 due to its nearby neighbour (Bachetti et al. 2020), the other three systems have been well-studied. Broad-band spectroscopy by Walton et al. (2018) found that the spectrum of NGC 7793 P13 was best fit by two soft components as well as a third, hard continuum component. X-ray spectroscopy of high cadence observations by Lin et al. (2022) found that NGC 7793 P13 has both a hard and a soft component, although it is unclear if the source's spectrum shows statistically significant changes over the observations.

Rodríguez Castillo et al. (2020) determined that M51 ULX7 was best fit by a black-body disc with a second (hotter) black-body model. A study of the source's spectral evolution by Brightman et al. (2022) found that there is not sufficient evidence for variation of the spectral shape either as a function of super-orbital phase or X-ray luminosity.

Studies of NGC 5907 ULX1 found that the source's spectrum was well characterised by a soft disc component with a power-law tail. Unlike the previous studies of the aforementioned ULXPs, spectral fits to observations of NGC 5907 ULX1 in 2003, 2012, and 2013 suggest that there is some evidence for spectral change as a function of phase (Fürst et al. 2017).

In the new MOOSE spectral monitoring of SMC X-1's high-state continuum, where we have probed a number of different super-orbital phases, we currently do not find strong evidence of intrinsic changes to SMC X-1's high-state continuum spectrum, although there may be some evidence for changes in N_H or Γ. Given that past studies have found that many systems find state changes linked to the mass transfer rate (Kotze & Charles 2012, and references therein), the lack of clear state changes during SMC X-1's excursion suggest that the relationship between the super-orbital period excursion and the high-state spectral parameters is somewhat complicated.

4 SUMMARY AND FUTURE STUDIES

We present the first full monitoring coverage which affords both high quality spectra and pulse profiles of SMC X-1 as it enters its fourth observed epoch of super-orbital period excursion.

Our initial findings are summarized as follows:

• We find that the new observations probe many different super-orbital phases and different super-orbital period values, and as such will provide a rich and diverse data-set that will be key to understanding the driving causes behind super-orbital period modulations.

• Fits to the spectral continuum are best-characterised by an absorbed black body disk with kT ~ 0.19 keV, and a hard power-law component (Γ ~ 0.7). Despite having probed different super-orbital periods and super-orbital period phases, we do not detect clear and significant evidence of changes to the continuum.

• We note a >3 σ increase in N_H (with kT relatively fixed) from the 2016 XMM-Newton observations to the 2021-2022 *NICER* monitoring, although this could be due to differences in the instruments (e.g. Schellenberger et al. 2015), rather than any physical changes.

• While the time averaged X-ray spectroscopy is a useful tool to make comparisons with other systems which may have similar accretion mechanisms, we see little evidence for spectral changes to the high-state as a function of super-orbital excursion.

• *NICER* monitoring of SMC X-1 via MOOSE will continue through early 2023. We will release all data products at the end of the monitoring period to cement the legacy value of this program.

The next step will be to perform a full study of pulse profiles (Brumback et al in prep), as well as phase-resolved spectroscopy and detailed study of any variability in the emission lines as a function of orbital and super orbital period, to delve into the physical origins of the super-orbital period modulation.

DATA AVAILABILITY

The *NICER* and *XMM-Newton* observations are publicly available on HEASARC, and the *Swift*/BAT (Krimm et al. 2013) lightcurves can be downloaded from https://swift.gsfc.nasa.gov/results/transients/SMCX-1/

REFERENCES

Bachetti M., et al., 2014, Nature, 514, 202
Bachetti M., et al., 2020, ApJ, 891, 44
Blondin J. M., Woo J. W., 1995, ApJ, 445, 889
Bonnet-Bidaud J. M., van der Klis M., 1981, A&A, 97, 134
Brightman M., et al., 2019, ApJ, 873, 115
Brightman M., et al., 2020, ApJ, 895, 127
Brightman M., et al., 2022, ApJ, 925, 18
Brumback M. C., Hickox R. C., Fürst F. S., Pottschmidt K., Tomsick J. A., Wilms J., 2020, ApJ, 888, 125
Clarkson W. I., Charles P. A., Coe M. J., Laycock S., Tout M. D., Wilson C. A., 2003a, MNRAS, 339, 447
Clarkson W. I., Charles P. A., Coe M. J., Laycock S., 2003b, MNRAS, 343, 1213
Corbet R. H. D., Krimm H. A., 2013, ApJ, 778, 45
Dage K. C., Clarkson W. I., Charles P. A., Laycock S. G. T., Shih I. C., 2019, MNRAS, 482, 337
Foulkes S. B., Haswell C. A., Murray J. R., 2006, MNRAS, 366, 1399
Foulkes S. B., Haswell C. A., Murray J. R., 2010, MNRAS, 401, 1275
Fürst F., Walton D. J., Stern D., Bachetti M., Barret D., Brightman M., Harrison F. A., Rana V., 2017, ApJ, 834, 77
Gendreau K. C., et al., 2016, in den Herder J.-W. A., Takahashi T., Bautz M., eds, Society of Photo-Optical Instrumentation Engineers (SPIE) Conference Series Vol. 9905, Space Telescopes and Instrumentation 2016: Ultraviolet to Gamma Ray. p. 99051H, doi:10.1117/12.2231304
Gruber D. E., Rothschild R. E., 1984, ApJ, 283, 546
Hickox R. C., Vrtilek S. D., 2005, ApJ, 633, 1064
Hu C.-P., Chou Y., Wu M.-C., Yang T.-C., Su Y.-H., 2011, ApJ, 740, 67
Hu C.-P., Chou Y., Yang T.-C., Su Y.-H., 2013, ApJ, 773, 58
Hu C.-P., Mihara T., Sugizaki M., Ueda Y., Enoto T., 2019, ApJ, 885, 123
Huang N. E., et al., 1998, Proceedings of the Royal Society of London Series A, 454, 903
Huijse P., Estévez P. A., Förster F., Daniel S. F., Connolly A. J., Protopapas P., Carrasco R., Príncipe J. C., 2018, ApJS, 236, 12
Hunter J. D., 2007, Computing in Science and Engineering, 9, 90
Inam S. Ç., Baykal A., Beklen E., 2010, MNRAS, 403, 378
Kaastra J. S., Bleeker J. A. M., 2016, A&A, 587, A151
Kotze M. M., Charles P. A., 2012, MNRAS, 420, 1575
Krimm H. A., et al., 2013, ApJS, 209, 14
Lin L. C.-C., Hu C.-P., Takata J., Li K.-L., Hui C. Y., Kong A. K. H., 2022, ApJ, 924, 65
Lucke R., Yentis D., Friedman H., Fritz G., Shulman S., 1976, ApJ, 206, L25
Marshall F. E., White N. E., Becker R. H., 1983, ApJ, 266, 814
Motch C., Pakull M. W., Soria R., Grisé F., Pietrzyński G., 2014, Nature, 514, 198
Naik S., Paul B., 2004, A&A, 418, 655
Neilsen J., Hickox R. C., Vrtilek S. D., 2004, ApJ, 616, L135
Ogilvie G. I., Dubus G., 2001, MNRAS, 320, 485
Paul B., Nagase F., Endo T., Dotani T., Yokogawa J., Nishiuchi M., 2002, ApJ, 579, 411
Pike S. N., et al., 2019, ApJ, 875, 144
Pradhan P., Maitra C., Paul B., 2020, ApJ, 895, 10
Pringle J. E., 1996, MNRAS, 281, 357
Remillard R. A., et al., 2021, arXiv e-prints, p. arXiv:2105.09901
Reynolds A. P., Hilditch R. W., Bell S. A., Hill G., 1993, MNRAS, 261, 337
Rodríguez Castillo G. A., et al., 2020, ApJ, 895, 60
Scargle J. D., 1982, ApJ, 263, 835
Schellenberger G., Reiprich T. H., Lovisari L., Nevalainen J., David L., 2015, A&A, 575, A30
Schreier E., Giacconi R., Gursky H., Kellogg E., Tananbaum H., 1972, ApJ, 178, L71
Thomas J. K., Charles P. A., Buckley D. A. H., Kotze M. M., Lasota J.-P., Potter S. B., Steiner J. F., Paice J. A., 2022, MNRAS, 509, 1062
Townsend L. J., Charles P. A., 2020, MNRAS, 495, 139
Trowbridge S., Nowak M. A., Wilms J., 2007, ApJ, 670, 624
van der Meer A., Kaper L., van Kerkwijk M. H., Heemskerk M. H. M., van den Heuvel E. P. J., 2007, A&A, 473, 523
van der Walt S., Colbert S. C., Varoquaux G., 2011, Computing in Science and Engineering, 13, 22
Vaughan S., Uttley P., Markowitz A. G., Huppenkothen D., Middleton M. J., Alston W. N., Scargle J. D., Farr W. M., 2016, MNRAS, 461, 3145
Verner D. A., Ferland G. J., Korista K. T., Yakovlev D. G., 1996, ApJ, 465, 487
Vrtilek S. D., Raymond J. C., Boroson B., McCray R., 2005, ApJ, 626, 307
Walton D. J., et al., 2016, ApJ, 827, L13
Walton D. J., et al., 2018, MNRAS, 473, 4360
Wilms J., Allen A., McCray R., 2000, ApJ, 542, 914
Wojdowski P., Clark G. W., Levine A. M., Woo J. W., Zhang S. N., 1998, ApJ, 502, 253
Wojdowski P. S., Clark G. W., Kallman T. R., 2000, ApJ, 541, 963

This paper has been typeset from a TeX/LaTeX file prepared by the author.